



Article

Extraction and Discrimination of MBT Anomalies Possibly Associated with the Mw 7.3 Maduo (Qinghai, China) Earthquake on 21 May 2021

Yuan Qi^{1,2}, Lixin Wu^{1,2,*}, Yifan Ding^{1,2}, Yingjia Liu^{1,2}, Shuai Chen^{1,2}, Xiao Wang^{1,2} and Wenfei Mao^{1,2}

¹ School of Geosciences and Info-Physics, Central South University, Changsha 410083, China; qiyuan_rs@csu.edu.cn (Y.Q.); 215001016@csu.edu.cn (Y.D.); liuyingjia@csu.edu.cn (Y.L.); s.chen1227@csu.edu.cn (S.C.); 215012193@csu.edu.cn (X.W.); maowenfei@csu.edu.cn (W.M.)

² Laboratory of Geo-Hazards Perception, Cognition and Predication, Central South University, Changsha 410083, China

* Correspondence: wulx66@csu.edu.cn

Abstract: Earthquakes are one of the most threatening natural disasters to human beings, and pre- and post-earthquake microwave brightness temperature (MBT) anomalies have attracted increasing attention from geosciences as well as remote sensing communities. However, there is still a lack of systematic description about how to extract and then discriminate the authenticity of seismic MBT anomalies. In this research, the first strong earthquake occurring near the northern edge of eastern Bayan Har block in nearly 20 years, the recent Mw 7.3 Maduo earthquake in Qinghai province, China on May 21, 2021, was selected as a case study. Based on the monthly mean background of MBT, the spatiotemporal features of MBT residuals with 10.65 GHz before and after the earthquake was firstly revealed. Referring to the spatial patterns and abnormal amplitudes of the results, four typical types of evident MBT positive residuals were obtained, and the time series of intensity features of each category was also quantitatively analyzed. Then, as the most influential factor on surface microwave radiation, air temperature, soil moisture and precipitation were analyzed to discriminate their contributions to these residuals. The fourth one, which occurred north to the epicenter after the earthquake, was finally confirmed to be caused by soil moisture reduction and thus ruled out as being related to seismicity. Therefore, the three retained typical MBT residuals with 10.65 GHz could be identified as possible anomalies associated with the Maduo earthquake, and were further analyzed collaboratively with some other reported abnormal phenomena related to the seismogenic process. Furthermore, through time series analysis, the MBT positive residuals inside the Bayan Har block were found to be more significant than that outside, and the abnormal behaviors of MBT residuals in the elevation range of 4000–5000 m reflected the shielding effect on microwave radiation from thawing permafrost on the plateau in March and April, 2021. This research provides a detailed technique to extract and discriminate the seismic MBT anomaly, and the revealed results reflect well the joint effect of seismic activity and regional coversphere environment on satellite-observed MBT.

Keywords: Maduo earthquake; microwave brightness temperature; monthly mean background; seismic thermal anomaly; Bayan Har block; coversphere environment



Citation: Qi, Y.; Wu, L.; Ding, Y.; Liu, Y.; Chen, S.; Wang, X.; Mao, W. Extraction and Discrimination of MBT Anomalies Possibly Associated with the Mw 7.3 Maduo (Qinghai, China) Earthquake on 21 May 2021. *Remote Sens.* **2021**, *13*, 4726. <https://doi.org/10.3390/rs13224726>

Academic Editor: Andrei Tronin

Received: 30 September 2021

Accepted: 20 November 2021

Published: 22 November 2021

Publisher's Note: MDPI stays neutral with regard to jurisdictional claims in published maps and institutional affiliations.



Copyright: © 2021 by the authors. Licensee MDPI, Basel, Switzerland. This article is an open access article distributed under the terms and conditions of the Creative Commons Attribution (CC BY) license (<https://creativecommons.org/licenses/by/4.0/>).

1. Introduction

At 18:04 on 21 May 2021 (UTC), the Mw 7.3 Maduo earthquake occurred at the southern Qinghai province, China, of which the epicenter was located at 34.59° N, 98.24° E, with a hypocenter depth of 10 km (USGS). This violent earthquake appeared inside the Bayan Har block, which is one of the representative active blocks of lateral extrusion in the Qinghai–Tibet Plateau since Cenozoic and one of the most intense areas of earthquake activity in China [1–3]. The Bayan Har block is enclosed by the East Kunlun fault zone as the north boundary, the Longmenshan fault zone as the east boundary, the Ganzi–

Yushu–Xianshuihe fault zone as the south boundary, and the Altun fault zone as the west boundary [1,4]. For the last 25 years, the strong earthquakes above Mw 6.5 (also above Ms 7.0) in mainland China all occurred on the faults around the Bayan Har block, including the 2001 Mw 7.8 western Kunlun Mountain earthquake, the 2008 Mw 7.2 and the 2014 Mw 6.9 Yutian earthquakes on the northern border, the 2008 Mw 7.9 Wenchuan earthquake, the 2013 Mw 6.6 Lushan earthquake and the 2017 Mw 6.5 Jiuzhaigou earthquake on the eastern border, and the 1996 Mw 6.9 Karakorum Mountain earthquake, the 1997 Mw 7.5 Manyi earthquake and the 2010 Mw 6.9 Yushu earthquake on the southern border of the Bayan Har block. The Maduo earthquake was located inside the Bayan Har block about 70 km south from the eastern Kunlun fault zone on the northern edge (see Figure 1), filling a spatial gap of earthquakes above Mw 6.5 in the middle-northern border [5].

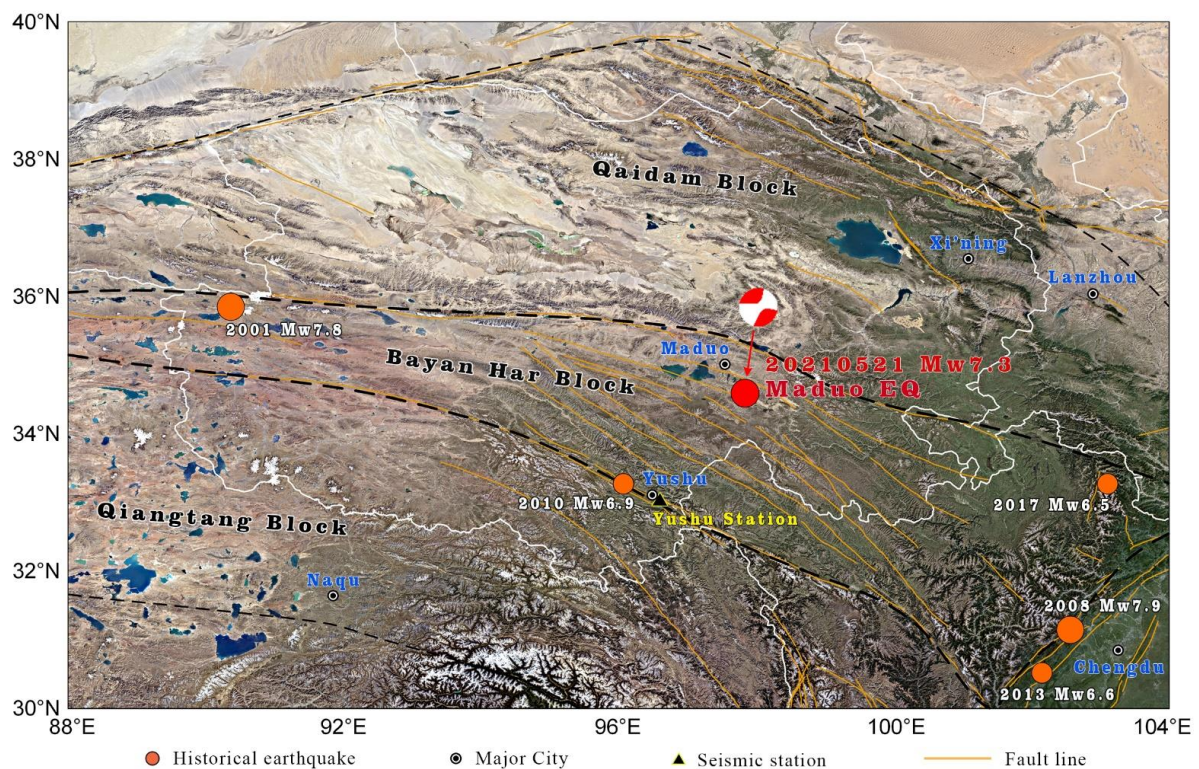


Figure 1. Visible image of the study area (from Google Earth). The red circle represents the epicenter of the Maduo earthquake, of which the focal mechanism was derived from the Global CMT Catalog. The orange circles stand for the historical large earthquakes ($M_w \geq 6.5$) in the study area.

According to field investigation after the mainshock and relocation study of after-shock sequence, the seismogenic fault of the Maduo earthquake was considered to be the Maduo–Gande fault, which is a sinistral strike-slip fault active in the Bayan Har block during Holocene, with a total length of 650 km [4–8]. Half a month after the earthquake, the USGS updated the slip distribution of the co-seismic rupture using broadband waveforms and finite fault model [9], and the coseismic deformation and displacements of the Maduo earthquake were inverted by Liu et al., [10] and Hua et al., [11] using SAR technology, and by Li et al., [12] using GNSS observations, the result showed that the co-seismic rupture length extended more than 140 km and the largest horizontal displacement was about 2–4 m, which was not far from the results of field surveys by Pan et al. [6]. In addition, Su et al., [13] reported that the well water temperature of Yushu seismic station (220 km away from the epicenter of Maduo earthquake) dropped abruptly in mid-March, 2021 and has since gradually returned to recover. Interference from instrumental performance, human activities and the natural environment were ruled out, and the mixing of the groundwater caused by stress-induced rock fracturing was considered as the potential cause of the abnormal water temperature decrease. Wang et al., [14] found that outgoing long-wave

radiation (OLR) anomalies north of the epicenter showed an expanding trend toward the epicenter with its amplitude strengthening before the earthquake and weakening after the earthquake. These abnormal phenomena on and under land surface reflected the different responses of crust stress change, and also indicated that there may be some observable anomalies before the earthquake.

Seismic thermal anomalies at the microwave band preceding some inland large earthquakes have been widely reported through numerous methods using different frequencies of microwave brightness temperature (MBT) data [15–24], and many characteristic results of geoscience significance have been obtained. Multi-source data, such as geological lithology, surface parameters, coversphere features and atmospheric remote sensing products, have been used to perform multi-parameter collaborative analysis involving MBT [18], and to further discriminate the authenticity of obtained MBT anomalies [22,25]. Theoretically, MBT depends on surface temperature and coversphere emissivity, the latter of which largely rely on dielectric properties and roughness of ground objects [26]. The passive microwave radiative signals emitting from the earth's surface are susceptible to many factors, in particular, to the terrain, vegetation, soil moisture, ice, snow and cloud cover [27]. The properties of surface medium will affect its microwave radiation capacity as radiation source in the form of low frequency dielectric and emissivity, while the existence of clouds will shield or add to the upward radiation at high frequency from earth surface [28]. Therefore, after the preliminary acquisition of MBT residuals before and after seismic activity, how to confirm or exclude the contributions of many sensitive factors to satellite MBT through reasonable processes and analysis methods, and then determine the MBT anomalies possibly related to earthquakes is very critical.

In this study, the spatiotemporal evolution of significant MBT positive residuals before and after the recent Maduo earthquake was revealed by removing the dynamic monthly-mean MBT background. Three types of abnormal MBT residuals featured with two positive strips and one positive spot, plus another large area of abnormal MBT positive residuals north to the epicenter were firstly obtained, and then the fourth type among them was identified as soil moisture decrease. After that, the authenticity of the retained MBT anomalies were discussed according to the seismogenic process of the Maduo earthquake. In addition, geological lithology, landcover, and DEM data were further employed to discuss the potential influence of seismogenic environment on satellite MBT and its residuals in the plateau area.

2. Methods and Materials

2.1. Monthly Mean Background

It is known that disturbances on ground surface and in the atmosphere can make the effective area of satellite observations highly uncertain. In particular, the high temporal variability of spatial location and thickness of clouds, and the uncertainty of particle size and distribution of water condensate in clouds will make it difficult to describe quantitatively the influence of clouds with models. Theoretically, passive microwave observation also depends on the incident angle, polarization, and frequency [29]. In general, common calibrated MBT products are selected for the study of information mining, thereby the effect of observation mode was not considered, hence the effective coverage of the data becomes a very important factor.

To acquire representative and complete MBT coverage over land, the satellite MBT is usually averaged over time series, hence the additive and shielding effect of clouds and some random disturbances can be smoothed out. Studies have shown that the optimum averaging period is about 30 days [27], during which averaging can achieve satisfactory results with the least amount of data. In this research, it is assumed that the mean of data 14 days before and 14 days after a given date in different years can represent the stable background of microwave radiation during the month of that date in a certain area or pixel. Therefore, when additional influence of seismic activity exists, the residuals with significant amplitude, obtained by removing the background MBT from target observation

containing the seismic increment, is deemed to be possibly related to the approaching earthquake. The MBT background ($MBTb$) and residual (ΔMBT) of each pixel is calculated as following:

$$MBTb_D = \frac{\sum_{y=m}^n \sum_{d=D-14}^{D+14} MBT_{y,d}}{N} \quad (1)$$

$$\Delta MBT_D = MBT_D - MBTb_D \quad (2)$$

where y and d represent the year and date of the MBT data for background construction, while $MBT_{y,d}$ refers to the MBT data on year y and date d in the study area. m and n stand for the start and end years of the available MBT datasets for the target month; N is the total number of valid data used in the same period of different years (not available every day due to the incomplete coverage of MBT swath). D represents the date of the target date to be studied before and after the seismogenic day, $MBTb_D$ is the MBT background on date D in the study area. MBT_D refers to original MBT of the target date D , and ΔMBT_D refers to the MBT residuals possibly associated with earthquake on date D .

Before implementing the construction of the monthly mean background, the study area, study time range and MBT data used should be determined in advance based on the target earthquake case. After the MBT residuals in the study area is obtained by removing the monthly mean background, the sensitive factors of satellite MBT need to be deeply analyzed (confirmed or ruled out) to determine the real cause of MBT anomaly. The analysis method of this study is shown in Figure 2.

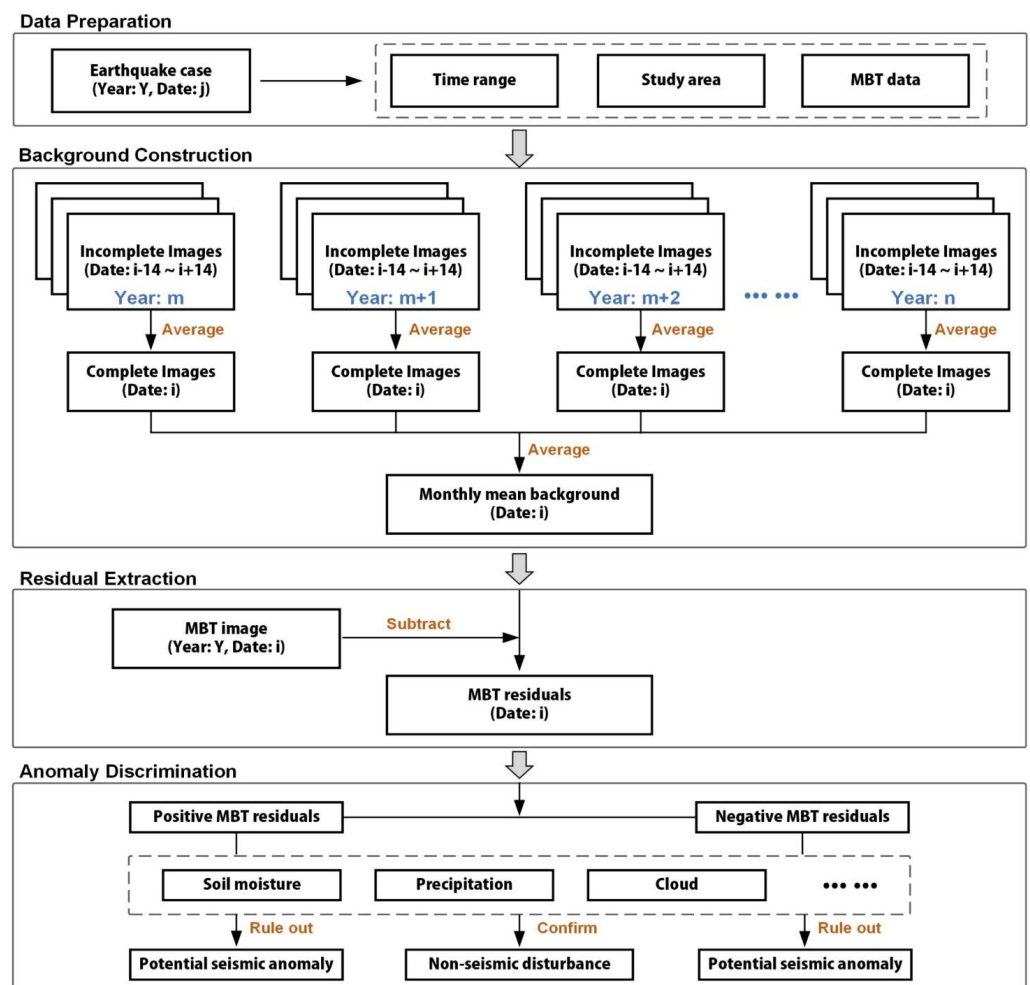


Figure 2. Analysis methodology of seismic microwave radiation anomaly based on monthly mean background of MBT.

2.2. Study Area

The investigated region of this research is selected as (30° N–40° N, 88° E–104° E), the vast majority of which is occupied by the Qinghai–Tibetan Plateau (see Figure 1). The study area completely covers the Qinghai Province, China, with four corners bordering Inner Mongolia, Gansu, Sichuan, Tibet and Xinjiang, China, respectively. Figure 1 shows the geolocations of the Mw 7.3 Maduo (Qinghai) earthquake on 21 May 2021 and some historical large earthquakes ($M_w \geq 6.5$) inside the study area. The complete list of historical large earthquakes around the Bayan Har block over the past 25 years are displayed in Table 1.

Table 1. Historical earthquakes of magnitude >6.5 in mainland China in the past 25 years.

Location	Time (UTC)	Magnitude (M _w)	Lat, Lon	Depth (km)
Karakorum Mountain pass	1996-11-19	6.9	35.35° N, 78.13° E	33
Manyi	1997-11-08	7.5	35.07° N 87.33° E	33
western Kunlun Mountain	2001-11-14	7.8	35.92° N 90.54° E	10
Yutian	2008-03-20	7.2	35.49° N 81.47° E	10
Wenchuan	2008-05-12	7.9	31.00° N 103.32° E	19
Yushu	2010-04-13	6.9	33.17° N 96.55° E	17
Lushan	2013-04-20	6.6	30.31° N 102.89° E	14
Yutian	2014-02-12	6.9	35.91° N 82.59° E	10
Jiuzhaigou	2017-08-08	6.5	33.19° N 103.86° E	9
Maduo	2021-05-21	7.3	34.60° N 98.25° E	10

The elevation in Figure 3a shows the particularity of terrain in the study area. The northern study area is composed of parallel ranges and valleys of the Altun and Qilian mountains, with an average elevation of over 4000 m. The Qaidam Basin northwest to the epicenter is a huge basin surrounded by the Altun, Qilian and Kunlun Mountains, which is 2600~3000 m above sea level with numerous lakes (mainly salt lakes) and swamps [30] in the south part. The central and southern study area is composed of Bayan Har block and Qiangtang block, with an average elevation of 4500 m. Figure 3b shows the geology in the study area. The Qaidam Basin locates to north of the Kunlun Mountains, the region south of the Altun mountains and Qilian Mountains outcrop the Tertiary and Quaternary strata, with its border running parallel to surrounding mountains. In the central part and southeast of the study area, an isosceles triangular Bayan Har fold system is characterized by widely distributed and well-developed Triassic deposits [31]. The southwestern part of the study area is dominated by unconformable contact between Jurassic and Cretaceous strata, which overlapped the Triassic [32]. Figure 3c shows the landcover distribution in the study area, while Figure 3d shows the proportion of each item of landcover in the study area. Grassland occupies the largest proportion with 59.12%, which is mainly found at altitudes above 3000 m. Bareland ranks second with a proportion of 25.12%, which is mainly distributed in the lower elevation area in the northern study area. The third largest area is forest, with a proportion of 6.56%, which grows mainly in the eastern end of Bayan Har block. These three categories of landcover occupy more than 90% of the study area.

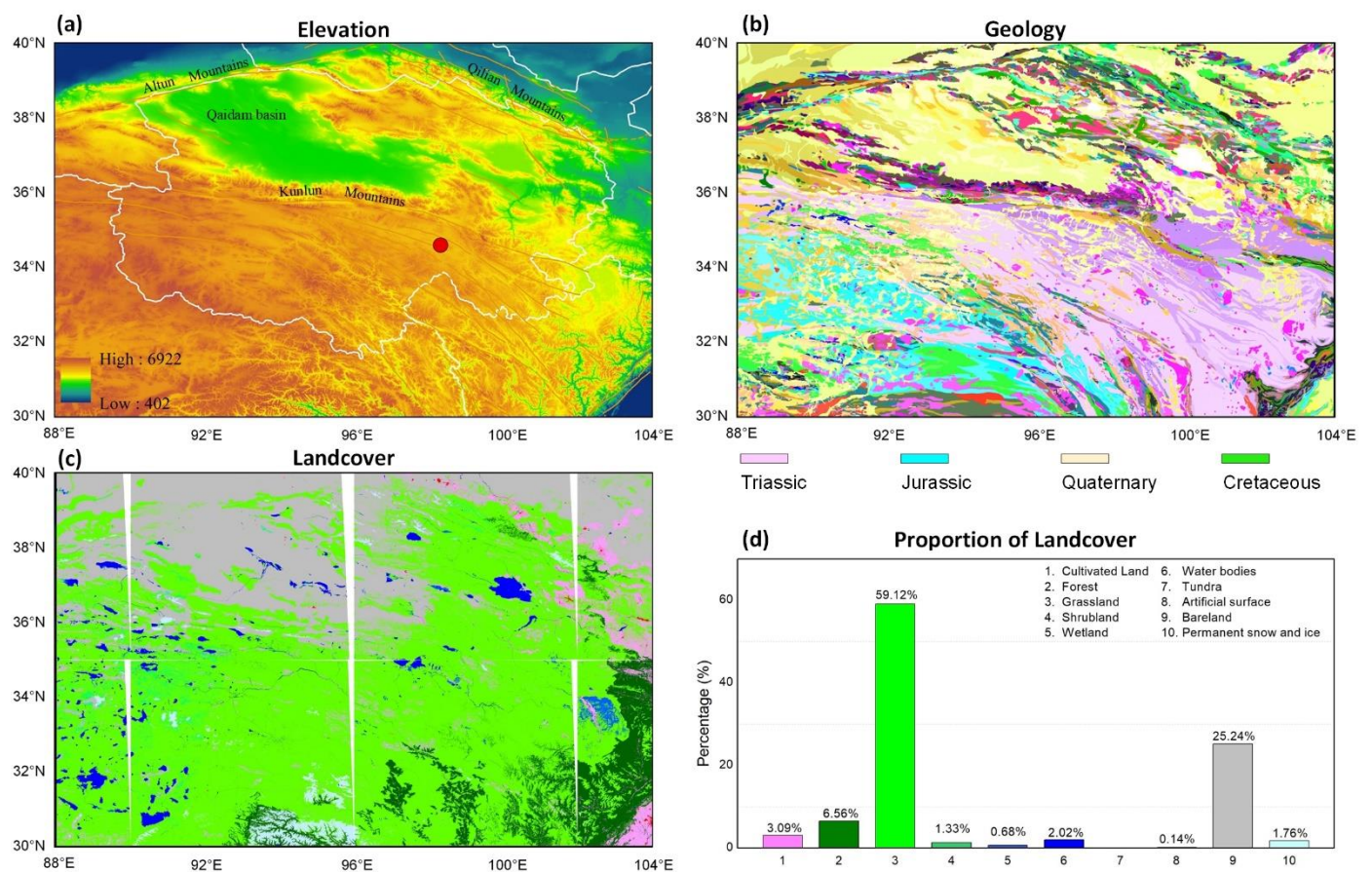


Figure 3. Distributions of elevation (a), geology (b), landcover and the proportion of each item (c,d) in the study area. The red circle in (a) represents the epicenter of the Maduo earthquake. The elevation is derived from SRTM-DEM dataset with 90 m resolution, the geological map is provided by 1:1 million spatial databases of geological maps of the People’s Republic of China [33], and the landcover data comes from the GlobeLand30 Dataset [34].

2.3. MBT Data

Since the 1960s, many remote sensing satellites for earth observation have been equipped with microwave radiometers. From then on, passive microwave remote sensing has become an important means to observe thermal radiation of the earth surface and exchange of surface energy [26]. The Special Sensor Microwave/Imager (SSM/I) onboard multiple generations of the Defense Meteorological Satellite Program (DMSP), the Advanced Microwave Scanning Radiometer-Earth Observing (AMSR-E) on NASA’s Aqua satellite, the Advanced Microwave Scanning Radiometer-2 (AMSR-2) on the Global Change Observation Mission-Water (GCOM-W1), and the MicroWave Radiation Imager (MWRI) onboard the Chinese meteorological satellite (FY-3B) have all been well used in the study of seismic microwave radiation anomalies [15,17,20,21,23]. Considering the occurring time of Maduo earthquake and the time coverage of available microwave data, the MBT data used in this study is selected from AMSR-2 instrument.

The AMSR-2 is designed as a successor of AMSR on the Advanced Earth Observing Satellite-II (ADEOS-II) and AMSR-E on board of Aqua satellite. Basic performance of AMSR2 is similar to that of AMSR-E but with several enhancements [35]. The instrument was launched in May 2012, and has been successfully collecting microwave radiation of the earth for more than nine years. The AMSR-2 has 12 channels, i.e., five microwave frequencies including 10.65, 18.7, 23.8, 36.5 GHz, and 89.0 GHz (A and B) at dual polarization (Vertical and Horizontal). The instantaneous field of view (IFOV) ranges from 24×42 km to 3×5 km (cross-track \times along-track), corresponding to the aforementioned five frequencies. The observation of AMSR-2 used in this study was obtained in descending

mode (local night time), to minimum the interferences from human activities and diurnal strong background. In this study, the entire time range of MBT data used is from June 2012 to August 2021. And, data from 2013 to 2021 were used to calculate MBT residual value from January to May, while data from 2012 to 2021 were used to calculate MBT residual value from June to July. The key parameters of the AMSR-2 are shown in Table 2.

Table 2. Major performances and characteristics of the AMSR-2 sensors.

Parameter		Performance					
Time of available data		June 2012–present					
Frequency (GHz)	10.65	18.7	23.8	36.5	89.0 A	89.0 B	
Polarization		H, V					
Spatial resolution (km)	50	25	25	15	5	5	
IFOV (cross-track × along-track, km)	42 × 24	22 × 14	26 × 15	12 × 7	5 × 3	5 × 3	
Band width (MHz)	100	200	400	1000	3000	3000	
Swath width (km)		1450					
NEΔT (K)		<0.7	<0.7	<0.6	<0.7	<1.2	<1.2
Measuring range (K)		2.7~340					
Incidence angle (°)	55.0	55.0	55.0	55.0	55.0	54.5	
Off-nadir angle (°)	47.5	47.5	47.5	47.5	47.5	47.0	

2.4. Auxiliary Data

In addition to the data shown in Figure 3, satellite remote sensing data such as soil moisture and precipitation are also used to conduct time series analysis and to discriminate the revealed MBT anomalies. Some information of the auxiliary data used in this research are shown in Table 3. Soil moisture and precipitation data are derived from NASA Global Land Data Assimilation (V.2.1) dataset, which is forced with a combination of Princeton meteorological forcing data model and observations from 2000 to present [36]. The value of soil moisture reflects the water content per square meter at depth 0–10 cm, while precipitation represents the total amount of precipitation obtained by multiplying the rate per second by three hours. The collection time of soil moisture is basically same as that of MBT data (18:00–21:00, UTC), while that of precipitation is 3 h earlier (15:00–18:00, UTC). Air temperature used in this study is represented by data of temperature at 2 m above the ground surface (T2M, in brief), which is provided by Copernicus Climate Change Service.

Table 3. Auxiliary data used in this research.

Data	Product	Spatial Resolution	Temporal Resolution	Unit	Website
Elevation	SRTM-DEM	90 m	/	meter	http://rmw.recordist.com/ (accessed on 9 July 2021)
Geology	Geological map	1:1 million	/	/	https://dcc.ngac.org.cn/ (accessed on 14 July 2021)
Landcover	GlobeLand30	30 m	/	/	www.webmap.cn/ (accessed on 28 July 2021)
Soil moisture	GLDA V.2.1	0.25°	3 h	kg/m ²	https://disc.gsfc.nasa.gov/ (accessed on 27 July 2021)
Precipitation	GLDA V.2.1	0.25°	3 h	kg/m ²	https://disc.gsfc.nasa.gov/ (accessed on 27 July 2021)
Air temperature	ERA5	0.1°	1 h	K	https://cds.climate.copernicus.eu (accessed on 15 November 2021)

3. Results

3.1. Spatiotemporal Features of the MBT Residuals

Figure 4 shows the retrieved MBT residuals, with 10.65 GHz at H polarization, from January to July, 2021, by using the method of monthly mean background. Overall, the study area was relatively quiet in January 2021, except for a few days with slight residuals to the south of the upcoming epicenter or in the northern margin of the study area. This indicates that in early 2021, the vicinity of the future epicenter was not the only area with stress response, and the northern edge of the Qaidam block may be the first to enter the state of stress concentration due to the continuous northward pushing of the Indian plate. From mid-late February, the central part of the study area began to show significant MBT positive residuals, which covered the forthcoming epicenter area and lasted until the end of March with gradually intensification. This strengthening of MBT residuals might correspond to the local stress starting to accumulate around Bayan Har block. In early April, the abnormal regions in the middle of the study area decreased sharply, only a small range of local positive and significant MBT residuals were found to the south of the epicenter. During this period, the plateau permafrost usually begins to thaw, and the resulting increment of soil moisture may overwhelm the MBT positive residuals around the future epicenter. In mid-late April and early May, significant MBT residuals reoccurred around the forthcoming epicenter, and their shapes appeared in strips or spots, but their intensity were slightly weaker than that in late March. This period has entered the late seismogenic phase of the impending Maduo earthquake, the stress near the forthcoming epicenter was highly concentrated, resulting in slight enhancement of MBT residuals even with the freeze-thaw effect. One week before the Maduo earthquake, more negative MBT residuals began to appear in the study area, and the scope of positive MBT residuals near the forthcoming epicenter was further reduced. As the rainy season on the plateau coming in June, the microwave radiation of surface soil was greatly affected. Therefore, on the day of the earthquake, there were no significant MBT positive residuals but negative residuals surrounding the epicenter. Several days after the earthquake, a large area of extremely obvious positive residuals began to occur in the area surrounding the Qaidam basin to the north of the epicenter, with its spatial position basically unchanged over time. The significant MBT positive residuals to the north of the epicenter remained conspicuous until the end of July, of which the scope and amplitude were enormously larger than that before the earthquake. Such post-earthquake MBT residuals with high amplitude are difficult to correspond spatially with potential stress concentration areas, and more auxiliary data are needed for further analysis.

According to the DTS criterion [37], these obtained residual values, which appeared near the occurrence date of the Maduo earthquake, had strong amplitudes and were adjacent to the epicenter area or the control faults, can be preliminarily identified as seismic anomalies. Then, some characteristic MBT residuals are picked out, which appeared alternately before and after the earthquake. According to their spatial locations and anomalous amplitudes, the revealed characteristic positive anomalies in Figure 4 can be divided into four categories. The first type was the abnormal strip of MBT positive residuals just along and covering the Bayan Har block (simply described as BHB strip), of which the spatial position and boundary of the strip were consistent with that of Bayan Har block. The BHB strip first appeared on 21 February, and peaked in strength on 18 and 19 April, with more distinct morphological features. The frequent occurrence of BHB MBT positive strip in this period proved that the response of in-situ stress was very active at this time. A few days before the earthquake, there were only slight traces with low intensity of BHB strip, due to the increased soil moisture from snow-ice thawing.

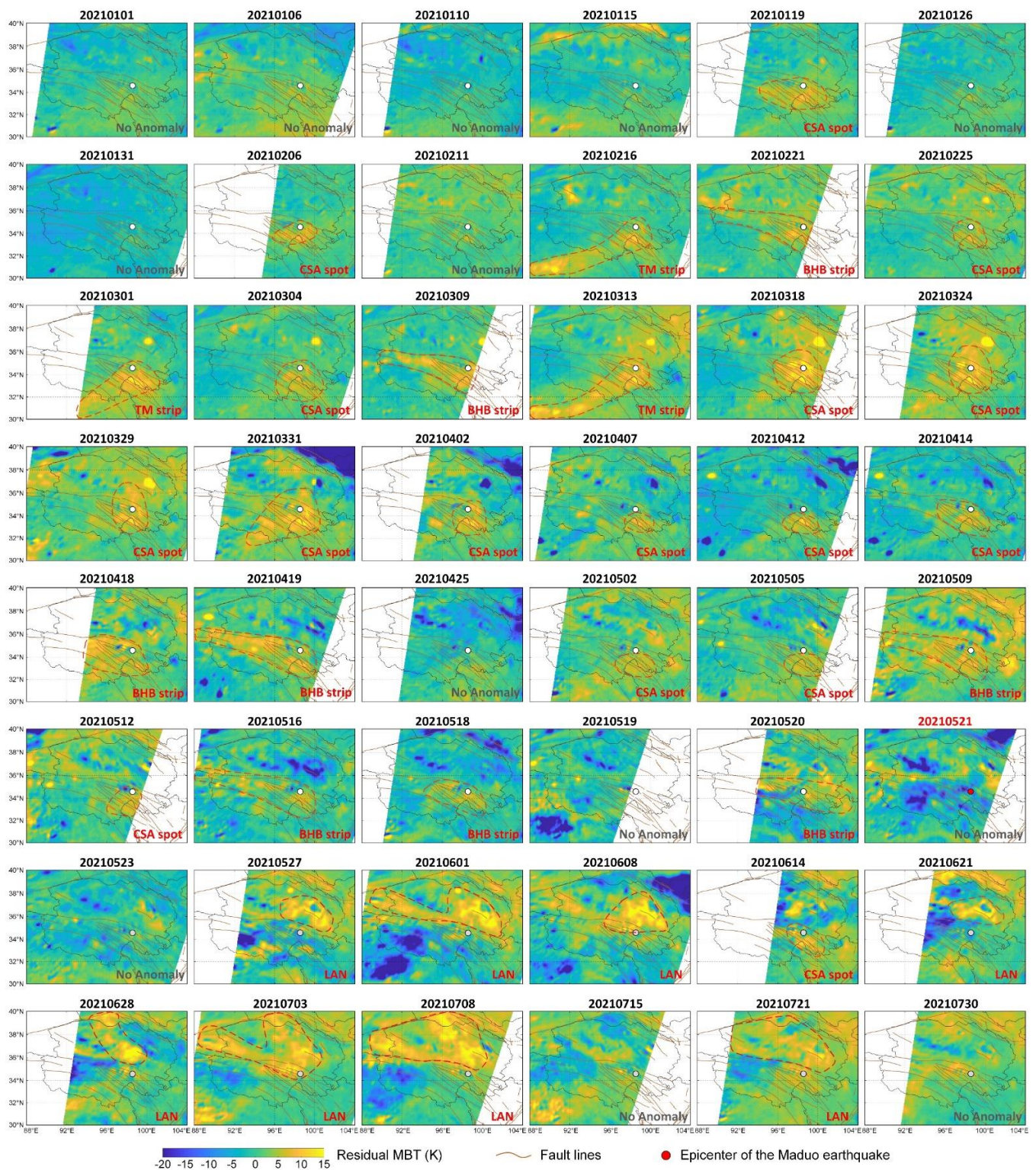


Figure 4. The retrieved MBT residuals (10.65 GHz at H polarization) in the study area from January to July, 2021. The circle dots mark the epicenter of the Maduo earthquake on 21 May 2021, with white, red, and gray color for the days before shock, on shock, and after shock, respectively. The text at the lower right corner of each subgraph indicates the type of residuals occurred on the day.

The second type was the abnormal strip of MBT positive residuals developed far away Maduo from Tibet (simply described as TM strip). The TM strip was very characteristic on 16 February and 13 March, which extended from the southwest corner of the study area

to the vicinity of the epicenter, presenting as an arc-shaped band. This strip was mainly presented in the first three months, and its shape might be related to the direction of local stress concentration.

The third type of abnormal MBT residuals was the regional spot-shaped anomaly covering or south adjacent to the epicenter (simply described as CSA spot), where the ends of the BHB strip and the TM strip overlapped. The CSA spot first appeared in 19 January, and its range and intensity changed with time and reached the peak in late March. In April and May, the occurrence of CSA spot was still very frequent, but the abnormal intensity was significantly reduced.

With regard to the above three types of abnormal MBT residuals, only CSA spot slightly appeared once after the earthquake. The fourth type was a large area of significant MBT residuals north to the epicenter (simply described as LAN), which located mainly to the southern boundary and in eastern region of Qaidam Basin. The LAN existed from the end of May and basically lasted throughout June to July, of which the shape changed gradually from a local spot north of the epicenter, to an obvious V-shape along the edge of the basin, with its intensity remaining high and reaching a peak on 8 July.

3.2. Time Series of Average Typical MBT Residuals

Figure 5 describes the type-time-intensity characteristics of different categories of MBT residuals from January to July, 2021. Figure A1 shows the four regions representing the range of the CSA spot, BHB strip, TM strip, and LAN, respectively. When doing the quantitative calculation, the valid values in the four ranges are firstly extracted according to the defined regions of the four typical MBT residuals, and then the obtained valid residuals are averaged. The histogram in Figure 5 represents the amplitude of the four typical abnormal MBT over time. Generally, the amplitude of CSA spot was relatively low in January to February, then peaked in March and weakened significantly in April. One month before the earthquake, the CSA spot had made another significant appearance. After the earthquake, there were significant and frequent negative values in June and some moderate positive outliers in July. The behavior of the BHB strip was similar to that of the CSA spot, but with slighter positive values and stronger negative values over time. The TM strip showed no significant abnormal behavior in the period of one month before the earthquake, and its amplitude in other periods was not so prominent. The LAN was active mainly after the earthquake, with the amplitude of positive and negative values both strong.

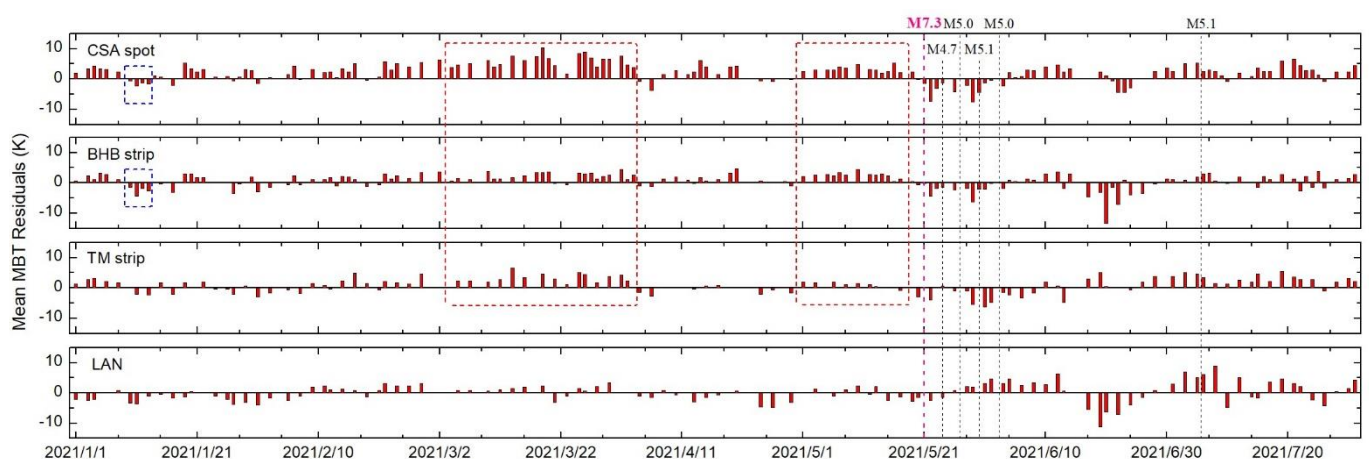


Figure 5. Time series of average residuals (10.65 GHz at H polarization) in the areas of four typical abnormal MBT defined in Figure A1 from January to July, 2021.

In mid-January, the blue boxes indicate several negative residuals, which may be related to regional snowfall in winter. Newly covered snow in permafrost regions might increase the overall surface permittivity of the depth that the microwave signal can penetrate, thereby reducing the local microwave radiation. The weakening effect of MBT in

April and May corresponded to the thawing of frozen soil on the plateau, the induced soil moisture rise reduced the surface microwave radiation. The negative values shortly after the earthquake and the significant drops in late June were mainly caused by the seasonal heavy rainfall (see Figure 6), and the potential impacts of numerous aftershocks were completely drowned out. The positive values of LAN in June and July might be associated with regional drought and strong surface evapotranspiration in summer (see Section 4.1), while the amplitude uplift of MBT residuals in CSA spot, BHB strip, TM strip might correlate with the impending strong aftershock (Mw 5.1) in early July.

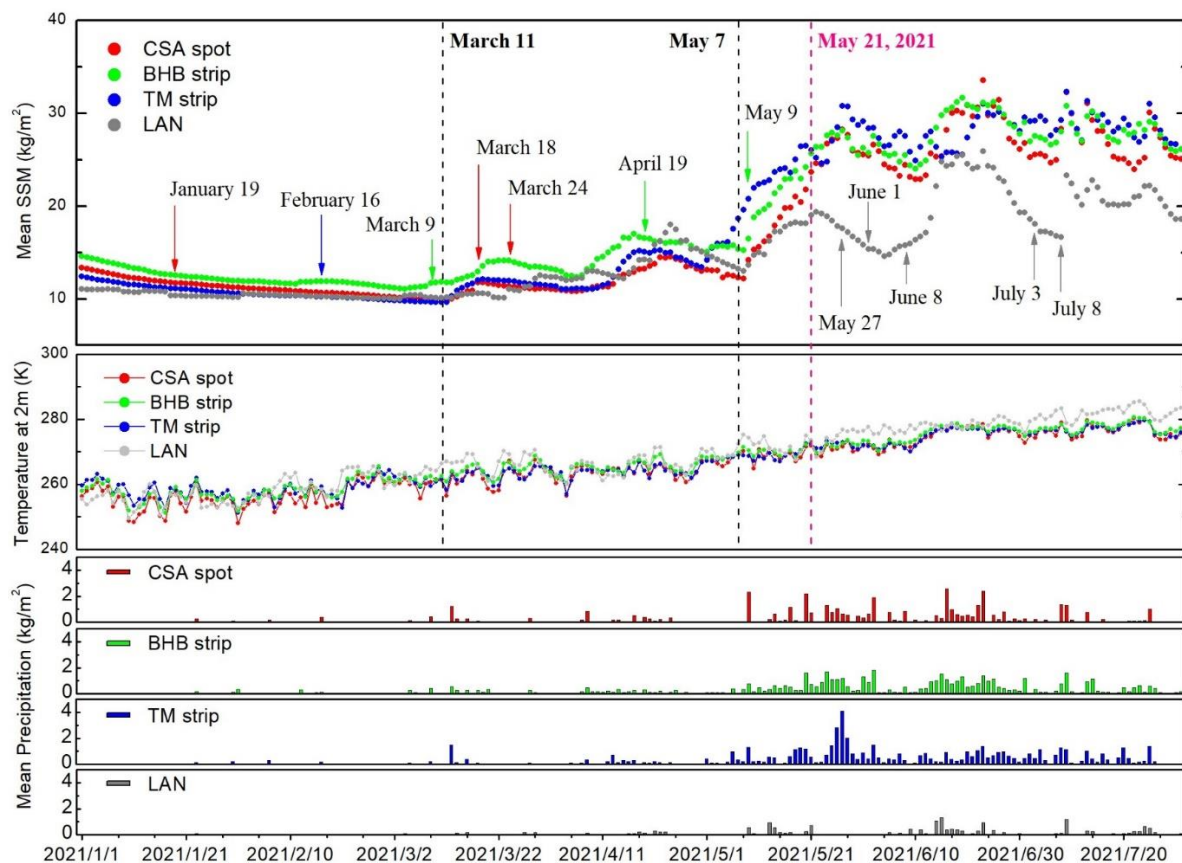


Figure 6. The variations of surface soil moisture, air temperature and precipitation in four characteristic abnormal regions from January to July, 2021. Several dates of the typical MBT residuals are indicated by arrows in the figure.

4. Analysis and Discussions

4.1. Analysis of the Influence of Soil Moisture

Theoretically, microwave radiation of the land surface is heavily affected by soil moisture through the influence of dielectric constant [38], and the disturbance of soil moisture in revealing seismic MBT anomaly has been discussed in previous studies [22,25]. As illustrated above, we obtain four typical abnormal MBT residuals before and after the Maduo earthquake, during the evolution process of which soil moisture seemed to be an important influencing factor in response to different environmental conditions, which still require further determination. In this study, the average variations of soil moisture, air temperature (T2M) and precipitation in the four areas defined in Figure A1 were calculated, the obtained results are shown in Figure 6.

According to the fluctuating amplitude, the changing process of soil moisture in Figure 6 can be roughly divided into three stages by two vertical dotted lines on 11 March and 7 May 2021, respectively. During the first stage (from 1 January and 11 March), the values of soil moisture in the four areas maintained low levels without obvious variation. It was still in the freezing period of surface soil on the Qinghai–Tibet plateau [39], the air

temperature was relatively low, so the material composition of land surface was relatively stable. In the second stage (from 11 March and 7 May), soil moisture in the four areas all ended its stable states, and began to rise slowly in a manner of fluctuation. During this period, although the precipitation in these areas were very little, the air temperature began to rise, and lead to the melting of surface frozen soil and in sequence a certain increase of surface soil moisture. During the third stage (from 7 May and 31 July), the soil moisture in the regions of CSA spot, TM strip and BHB strip increased dramatically due to the precipitation, but that of LAN diverged from the other three regions due to much fewer precipitation. After the earthquake on 21 May, the air temperature of LAN was relatively higher and behaved negatively correlated with the soil moisture. Meanwhile, several continuous peaks and troughs of soil moisture of LAN was consistent with the presence and absence of precipitation in the LAN in June and July, 2021.

In Figure 6, three arrows in the first stage indicate the date when the CSA spot, TM strip and BHB strip appeared on 19 January, 16 February and 9 March, respectively. Soil moisture and air temperature in this period were relatively low and stable, which was not high enough to cause significant changes in microwave radiation. Therefore, the significant MBT residuals in these days were more like to be associated with the future mainshock. In the second stage, the thawing process of the snow-ice as well as frozen soil had lifted the surface soil moisture, which was in principle a depressant effect on the microwave radiation of shallow soil. However, in the days such as 18 March, 24 March and 19 April, there were still very evident MBT positive residuals, which means that the positive impact on microwave radiation possibly related to the upcoming Maduo earthquake was not thoroughly drown by the negative impact on microwave radiation due to increase in surface soil moisture. This period might correspond to the locking stage of crust stress before the Maduo earthquake, thus showing a relatively strong microwave radiation response. In the third stage, with the arrival of rainy season on the plateau, regional precipitation and soil moisture increased substantially, which greatly weakened the positive impacts of seismogenic activity, thereby the MBT positive residuals stayed at relatively low levels in early-to-mid- May (as in Figure 4). However, the MBT positive residuals near the epicenter were sometimes still significant several days before the shocking day, such as 9 May, which might also be influenced by the upcoming strong earthquake. After 21 May (the shocking day), soil moisture in the area of LAN fluctuated at low level and was extremely sensitive to changes in precipitation. High MBT positive residuals in the days of 27 May, 8 June, 3 July and 8 July all corresponded well to the lack of precipitation and high air temperature. This consistency means that the MBT positive residuals in large area north to the epicenter (LAN) after the earthquake was mainly caused by reduction of surface soil moisture instead of subsequent seismic activity.

4.2. Time Series Analysis of MBT and Its Residuals

In the previous research, the intrinsic relationship between MBT anomaly and geological condition [22], coversphere features [40] and terrain features [23] has been studied, which illustrates the decisive influence of seismogenic environment on MBT anomaly. In this study, the mean value of MBT and its positive residuals (10.65 GHz, H-pol), soil moisture and air temperature changing with time inside and outside the Bayan Har block (Figure 7a), inside and outside the Quaternary strata (Figure 7b), in different elevation intervals (Figure 7c), and in different landcover areas (Figure 7d) were calculated, in order to analyze the potential impacts from seismogenic environment and regional coversphere on the MBT and its positive residuals.

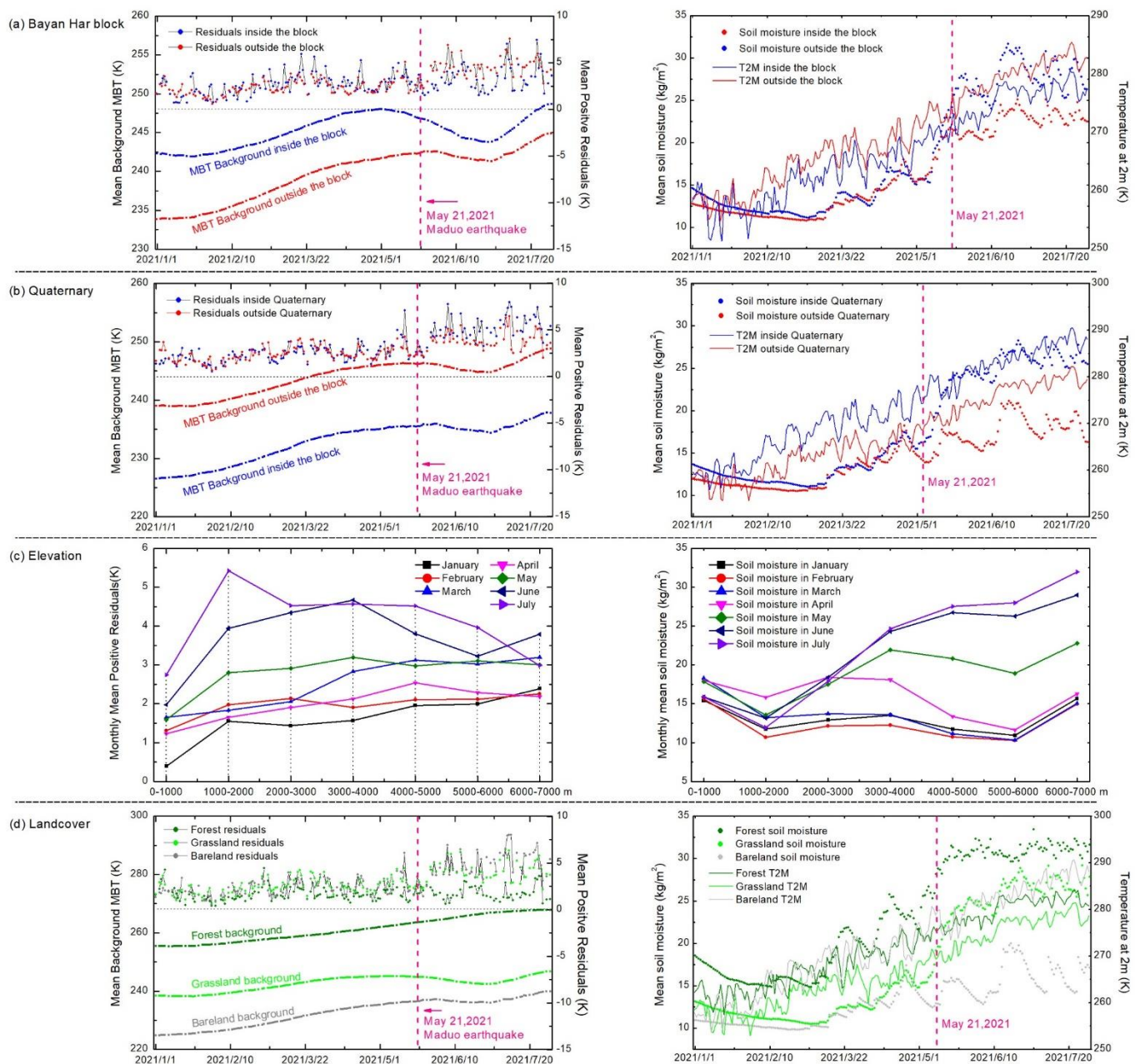


Figure 7. Time series of background MBT and average MBT positive residuals with 10.65 GHz at H polarization (left), soil moisture and air temperature (right), inside and outside the Bayan Har block (a), in and outside the Quaternary regions (b), of different elevation intervals (c), and in different landcover regions (d).

In the left subgraph of Figure 7a, the two vertical axes represent the average of the original MBT observations (left) and the residual values after removing the monthly mean background (right) in the respective area. The average background MBT inside the Bayan Har block was slightly higher than that outside, which may be due to the differences in soil moisture, land features and average altitudes in the two regions. In the right subgraph of Figure 7a, the mean values of soil moisture outside the Bayan Har block is slightly higher than that inside before May 2021, and the sharply rise in soil moisture in June and July, which was caused by seasonal precipitation in the plateau area, explains the significant decrease of MBT background. Meanwhile, the average MBT positive residuals inside the Bayan Har block was also generally higher than that outside from January to May, especially on 20 January, 26 March, and 19 April (corresponding to result in Figures 4 and 5). The difference between the curves inside and outside the block may

indicate that the significant MBT positive residuals were more inclined to appear inside the Bayan Har block before the Maduo earthquake, which might be related to the seismogenic preparation of the impending mainshock. In June to July, the difference in residual MBT was due to the dramatical variation of soil moisture (see the right subgraph). What follows was a significant change in dielectric constant of the surface, which led to frequent significantly reduction in MBT residuals with precipitation and rise in MBT residuals without precipitation after the earthquake.

In Figure 7b, the curves inside and outside the Quaternary region differ only in the average background MBT but not in the MBT positive residuals. It is air temperature and soil moisture that both contributed to this difference. The result shows that the tendency of significant MBT residuals to Quaternary (once appeared in Wenchuan earthquake [22]) was not reflected in the Maduo earthquake, which might be related to the shielding effect of the specific seismogenic environment and extremely fickle coversphere. The overall trend of background MBT inside and outside the Quaternary region behaved similarly. After the earthquake, the values of soil moisture inside and outside the Quaternary region increased sharply and fluctuated dramatically in June and July, which was the reason for the depression of background MBT and the unstable state of MBT residuals after the mainshock.

Figure 7c shows the monthly average of MBT positive residuals and soil moisture in seven elevation intervals. With the increase of altitude, the mean values of MBT residuals generally showed an upward trend in January to May. In June to July, the MBT residuals increased in the range of 0–2000 m, and decreased significantly above 2000 m, which was highly negatively correlated with the variation of soil moisture in the right subgraph. This might be owing to the thawing process in high-altitude areas caused by the increase of air temperature on the plateau in summer. For areas with the same level interval, the MBT residuals generally increased from January to July, but in March and April there was an opposite trend, especially in the 4000–6000 m range, where was consistent with those of the seasonal frozen soil area on Qinghai plateau in elevation and space [41]. This consistency can be confirmed by the decreasing in soil moisture in the same elevation range from January to May. Therefore, the discontinuous trend exhibited in Figure 7b could be attributed to the thawing permafrost on the plateau, which resulted in the significant increment of soil moisture and surface dielectric, and in turn reduced the surface microwave radiation. The revealed results show that surface microwave radiation is very sensitive to the change of external seismogenic environment.

In Figure 7d, only three landcovers with high proportions (grassland, bare land, and forest) were considered. Referring to the elevation and landcover in Figure 3 and the variation of air temperature in the right subgraph, the differences in average background MBT of the three landcovers were caused by the combination of air temperature and emissivity of the land surface. The curve of forest showed a continuous upward trend from January to July, which was due to the growth of vegetation in low altitude region and the increasing volume scattering of forest to MBT. The background MBT and soil moisture in the forest area both stayed at the highest level, and the increase of soil moisture after May positively promoted the growth of vegetation, and then encouraged the microwave scattering of vegetation to dominate. The curve of grassland began to rise with air temperature in January and reached an inflection point in April, which was due to the increasing in soil moisture caused by thawing process in the frozen soil region. The grassland grew luxuriant in summer, but the low-frequency microwave radiation mainly reflects the increase of soil moisture in the grassland area, so the background MBT of the grassland decreased in June and July. As for the bare land, the trend of background MBT curve behaved similar to that of grassland but with a low level. Although the soil moisture in the bare land area was relatively low and air temperature was high, its microwave emissivity was much lower than vegetated areas, thus the MBT was weaker. For the three typical landcovers, there existed no obvious difference in MBT residuals from January to May, but the MBT residuals of forest region showed a stable state without response to soil moisture change

after the earthquake, which further indicates that the change of surface dielectric properties in forest area (caused by soil moisture change) is not the main factor affecting MBT in this area. The features of background MBT in forest and grassland areas reflect the effect of seismogenic environment and the response of MBT to phenology.

4.3. Analysis of the MBT Positive Anomalies

Generally, low frequency MBT data is considered to be a good reflection of surface microwave radiation. After removing the disturbance of soil moisture and precipitation, the remaining three types of MBT residuals with 10.65 GHz, i.e., the CSA spot, BHB strip and TM strip, can be considered as seismic MBT anomalies related to the Maduo earthquake.

Referring to the overall tectonic movement trend of the Qinghai–Tibet Plateau [1], the early anomaly to north of the Qilian mountains and the Altun mountains in January might reflected the stress adjustment in northern margin of the plateau, which then might had led to the following positive CSA spot on 19 January and 6 February. The positive TM strip on 16 February might be a response to the direction of plate extrusion and stress concentration. Then the positive BHB strip and TM strip started to alternate over time, and three abnormal species became extremely significant in mid-late March, which was at the same period as the underground water temperature anomaly [13]. This synchronous change suggests that block tectonics near the epicenter might have become very active during this period. In the first half of April, there were only slight anomalies around the forthcoming epicenter, which was confirmed to be owing to thawing permafrost on the plateau. Meanwhile, the regional load/unload response ratio (LURR) was found to change dramatically one month before the Maduo earthquake, and OLR anomaly occurred to the north of the epicenter with a trend of expanding toward the epicenter and strengthening before the earthquake [14], which further confirmed that the variation of crustal stress was capable of arousing some thermal responses on the earth's surface during the late phase of earthquake preparation. In addition, Wang et al. [14] suggested that the crustal medium might reach the end of the yield phase and start the fracturing-to-failure stage from one month before the earthquake, which means that the seismogenic system gradually tended to be unstable. Therefore, it is reasonable that we obtained significant positive anomalies occurring near the epicenter (CSA spot) on 14 April and pervading the Bayan Har block on 18 and 19 April (BHB strip). Half a month before the earthquake, the anomalies were mainly focused near the epicenter (CSA spot) and distributed along the Bayan Har block (BHB strip), with the amplitude still to be visible even seriously disturbed by seasonal precipitation. This indicates that crustal stress was more concentrated shortly before the earthquake, and the induced MBT anomalies were strong enough to not be completely drown by the precipitation. By the end of May, seismic activity in the study area became weak, and the rainy season was coming on the plateau, so that the central part of the study area returned to calm even to be negative state in this period. The CSA spot occurred once after the earthquake, which might be related to a strong aftershock in the Qaidam basin on 14 June. The evolution process of positive MBT anomalies from January to May basically reflected the joint effect of crustal stress and seismogenic environment and regional coversphere on surface microwave radiation.

As for the remote sensing physics of the positive MBT anomaly, a chain reaction (crust stress change–charge carrier accumulation–surface dielectric reduction) based on laboratory experiments and theoretical analysis [22,42–44] can be invoked. The extrusion from the Indian plate and the blocking of the Qaidam block, coupled with the existence of many secondary faults in the Bayan Har block and the Qiangtang block, caused the internal and boundary displacement of the blocks in the late phase of earthquake preparation, which created a favorable condition for the aforementioned chain reactions. Furthermore, previous studies have also revealed thermal anomalies preceding the Yushu earthquake, which was another powerful earthquake occurred on the southern margin of the Bayan Har block on 13 April 2010. A case in point is that a strip-shaped thermal infrared anomaly occurred on 17 March 2010 [45] and a strip of positive MBT anomaly occurred on 5 April 2010 [24],

which had similar characteristics in shape and location, and were found to be all confined by the tectonic faults. These particular phenomena indicate that there may exist a commonality of pre-earthquake thermal anomalies within the Bayan Har block, which deserves further studies.

5. Conclusions

The Earth system is far from equilibrium [46], and the seismogenic environment varies with its special spatial location, so the surface microwave radiation observed by satellites is vastly different and inevitably affected by many factors. The major disturbances to the earth's surface, from which the microwave radiation emits, need to be eliminated one by one before the obtained MBT residuals can be considered to be seismic anomalies, and then the MBT anomaly should be analyzed from the perspective of seismogenic process. In this research, by selecting the Maduo (Qinghai, China) earthquake as a nice case study, the spatiotemporal evolution of MBT residuals with 10.65 GHz from January to July, 2021 were revealed, by using MBT data from AMSR-2 instrument. The extracting method of the monthly mean background and the discriminating on MBT residuals using multiple dataset were implemented combined with the obtained results.

Referring to the features of shape and intensity, four typical types of significant MBT positive residuals were firstly found before and after the Maduo earthquake, including a strip-shaped abnormal MBT overlapping with the Bayan Har block, an arcuate strip-shaped abnormal MBT developed from Tibet to Maduo county, a regional abnormality covering or south adjacent to the epicenter where the ends of the two strips overlapped, and a large area of positive residuals north to the epicenter after the earthquake. Time series of the four MBT positive residuals were also quantitatively analyzed. Then, by analyzing the temporal variations of quasi-synchronous air temperature, soil moisture and precipitation, the large area of abnormality north to the epicenter were identified to be caused by soil moisture reduction in June and July, the retained three MBT residuals were considered to be possibly associated with the Maduo earthquake.

In addition, in order to analyze the potential influence of seismogenic environment and regional coversphere in the plateau region, time series of averaged background MBT together with the residual MBT in different regions was further analyzed, by using auxiliary data including elevation, geological map, landcover and soil moisture. The results show that the MBT positive residuals were more pronounced inside the Bayan Har block than that outside before the earthquake. In the elevation range of 4000–5000 m, the obtained MBT residuals reflected the weakening influence of permafrost thawing on microwave radiation in March and April, 2021. The effect of tectonic block and plateau thawing on MBT has been fully emphasized according to the results in this study, but the influences of geology and landcover on the MBT and its residuals were considered to actually originate from air temperature and phenology of vegetation. Finally, referring to seismogenic process of the Maduo earthquake, the spatiotemporal features and potential causes of the remaining three MBT anomalies were jointly analyzed and briefly discussed.

Taking the recent Mw 7.3 Maduo earthquake on 21 May 2021 as an example, this study elaborated the detailed analysis method and idea of seismic MBT anomaly from the aspects of data selection, monthly mean background establishment, residual MBT extraction and seismic anomaly discrimination. The analysis and discussion on the MBT anomaly of the Maduo earthquake have a guiding significance for understanding the special influences of seismogenic environment on satellite MBT in the Qinghai–Tibet Plateau region.

Author Contributions: Conceptualization, Y.Q.; data curation, Y.D., Y.L., S.C. and X.W.; formal analysis, L.W. and W.M.; funding acquisition, L.W.; methodology, Y.Q.; validation, Y.D., Y.L., S.C. and W.M.; visualization, Y.D. and Y.L.; writing—original draft, Y.Q.; writing—review and editing, Y.Q. and L.W. All authors have read and agreed to the published version of the manuscript.

Funding: This research was funded by the National Key R & D Program of China, grant number 2018YFC15035, the Key Program of the National Natural Science Foundation of China, grant number

41930108, the innovation leading program of Central South University, grant number 506030101, and the Talents Gathering Program of Hunan Province, China, grant number 2018RS3013.

Data Availability Statement: MBT data: <https://disc.gsfc.nasa.gov/datasets> (accessed on 9 July 2021); Other data: See Table 3.

Acknowledgments: MBT data, soil moisture data and precipitation data were acquired and owned by Goddard Earth Sciences Data and Information Services Center. Air temperature data were acquired and owned by Copernicus Climate Change Service. Landcover data were acquired and owned by National Catalogue Service for Geographic Information.

Conflicts of Interest: The authors declare no conflict of interest.

Appendix A

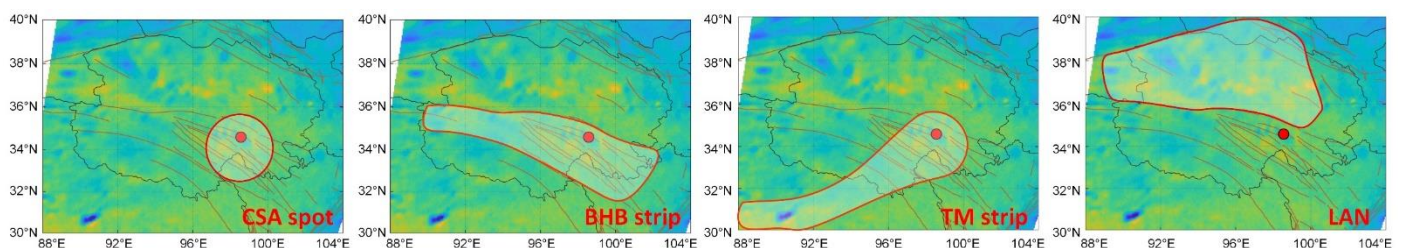


Figure A1. The four areas used to calculate the mean MBT residuals of the CSA spot, BHB strip, TM strip and LAN, respectively.

References

- Zhang, P.Z.; Deng, Q.D.; Zhang, G.M.; Ma, J.; Gan, W.J.; Min, W.; Mao, F.Y.; Wang, Q. Active tectonic blocks and strong earthquakes in the continent of China. *Sci. China Earth Sci.* **2003**, *46*, 13–24. [\[CrossRef\]](#)
- Zhang, P.Z.; Shen, Z.; Wang, M.; Gan, W.J.; Burgmann, R.; Molnar, P. Continuous deformation of the Tibetan Plateau from global positioning system data. *Geology* **2004**, *32*, 809–812. [\[CrossRef\]](#)
- Xu, R.; Sarah, D.S. Present-day kinematics of the eastern Tibetan Plateau and Sichuan Basin: Implications for lower crustal rheology. *J. Geophys. Res. Solid Earth* **2016**, *121*, 3846–3866. [\[CrossRef\]](#)
- Chen, C.Y.; Ren, J.W.; Meng, G.J.; Yang, P.X.; Xiong, R.W.; Hu, C.Z.; Su, X.N.; Su, J.F. Division, deformation and tectonic implication of active blocks in the eastern segment of Bayan Har block. *Chin. J. Geophys.* **2013**, *56*, 4125–4141. [\[CrossRef\]](#)
- Wang, W.L.; Fang, L.H.; Wu, J.P.; Tu, H.W.; Chen, L.Y.; Lai, G.J.; Zhang, L. Aftershock sequence relocation of the 2021 MS7.4 Maduo Earthquake, Qinghai, China. *Sci. China Earth Sci.* **2021**, *64*, 1371–1380. [\[CrossRef\]](#)
- Pan, J.W.; Bai, M.K.; Li, C.; Liu, F.C.; Li, H.B.; Liu, D.L.; Marie, L.; Wu, K.G.; Wang, P.; Lu, H.J.; et al. Coseismic surface rupture and seismogenic structure of the 2021-05-22 Maduo (Qinghai) Ms7.4 earthquake. *Acta Geol. Sin.* **2021**, *95*, 1655–1670. [\[CrossRef\]](#)
- Yin, X.X.; Wang, W.H.; Cai, R.; Deng, J.; Ma, L. Precise location of the 2021 Maduo, Qinghai Ms7.4 earthquake and its seismogenic structure. *China Earthq. Eng. J.* **2021**, *43*, 834–839.
- Zhan, Y.; Liang, M.J.; Sun, X.Y.; Huang, F.P.; Zhao, L.Q.; Gong, Y.; Han, J.; Li, C.X.; Zhang, P.Z.; Zhang, H.P. Deep structure and seismogenic pattern of the 2021.5.22 Madoi (Qinghai) MS7.4 earthquake. *Chin. J. Geophys.* **2021**, *64*, 2232–2252. [\[CrossRef\]](#)
- Cross-Section of Slip Distribution of M7.3 Maduo Earthquake. Available online: <https://earthquake.usgs.gov/earthquakes/eventpage/us7000e54r/finite-fault> (accessed on 10 August 2021).
- Liu, J.H.; Hu, J.; Li, Z.W.; Ma, Z.F.; Wu, L.X.; Jiang, W.P.; Feng, G.C.; Zhu, J.J. Complete three-dimensional coseismic displacements due to the 2021 Maduo earthquake in Qinghai Province, China from Sentinel-1 and ALOS-2 SAR images. *Sci. China Earth Sci.* **2021**, in press. [\[CrossRef\]](#)
- Hua, J.; Zhao, D.Z.; Shan, X.J.; Qu, C.Y.; Zhang, Y.F.; Gong, W.Y.; Wang, Z.J.; Li, C.L.; Li, Y.C.; Zhao, L.; et al. Coseismic deformation field, slip distribution and coulomb stress distribution of the 2021 Mw7.3 Maduo earthquake using sentinel-1 InSAR observations. *Seismo. Geol.* **2021**, *43*, 677–691. [\[CrossRef\]](#)
- Li, Z.C.; Ding, K.H.; Zhang, P.; Wen, Y.M.; Zhao, L.J.; Chen, J.F. Co-seismic deformation and slip distribution of 2021 Mw 7.4 Maduo earthquake from GNSS observation. *Geom. Inf. Sci. Wuhan Univ.* **2021**, *46*, 1489–1497. [\[CrossRef\]](#)
- Su, W.G.; Liu, L.; Yuan, F.Q.; Zhao, Y.H.; Sun, X.H. The anomaly characteristics of well water temperature in Yushu seismic station before the 2021 Maduo MS7.4 earthquake. *Acta Geol. Sin.* **2021**, *43*, 1–5. [\[CrossRef\]](#)
- Wang, S.Y.; Tian, H.; Ma, K.X.; Yu, C.; Ma, W.Y.; Yu, H.Z. Correlation between short-term and imminent anomalies of LURR and OLR before the Maduo Ms7.4 earthquake in Qinghai Province. *China Earthq. Eng. J.* **2021**, *42*, 847–852.
- Takashi, M.; Takano, T. Detection algorithm of earthquake-related rock failures from satellite-borne microwave radiometer data. *IEEE Trans. Geosci. Remote Sens.* **2010**, *48*, 1768–1776.
- Chen, H.; Jin, Y.Q. A preliminary detection of anomalous radiation of rock failures related with Yushu earthquake by using satellite-borne microwave radiometers. *Remote Sens. Technol. Appl.* **2010**, *25*, 860–866. [\[CrossRef\]](#)

17. Singh, R.P.; Mehdi, W.; Gautam, R.; Kumar, J.S.; Zlotnicki, J.; Kafatos, M. Precursory signals using satellite and ground data associated with the Wenchuan earthquake of 12 May 2008. *Int. J. Remote Sens.* **2010**, *31*, 3341–3354. [CrossRef]
18. Jing, F.; Singh, R.P.; Shen, X. Land-atmosphere-meteorological coupling associated with the 2015 Gorkha (M 7.8) and Dolakha (M 7.3) Nepal earthquakes. *Geomat. Nat. Hazards Risk* **2019**, *10*, 1267–1284. [CrossRef]
19. Jing, F.; Singh, R.P.; Sun, K.; Shen, X. Passive microwave response associated with two main earthquakes in Tibetan Plateau, China. *Adv. Space Res.* **2018**, *62*, 1675–1689. [CrossRef]
20. Jing, F.; Singh, R.P.; Cui, Y.; Sun, K. Microwave brightness temperature characteristics of three strong earthquakes in Sichuan province, China. *IEEE J. Sel. Topics Appl. Earth Observ. Remote Sens.* **2020**, *13*, 513–522. [CrossRef]
21. Qi, Y.; Wu, L.X.; He, M.; Mao, W.F. Spatio-temporally weighted two-step method for retrieving seismic MBT anomaly: May 2008 Wenchuan earthquake sequence being a case. *IEEE J. Sel. Topics Appl. Earth Observ. Remote Sens.* **2020**, *13*, 382–391. [CrossRef]
22. Qi, Y.; Wu, L.X.; Mao, W.F.; Ding, Y.F.; He, M. Discriminating possible causes of microwave brightness temperature positive anomalies related with May 2008 Wenchuan earthquake sequence. *IEEE Trans. Geosci. Remote Sens.* **2021**, *59*, 1903–1916. [CrossRef]
23. Qi, Y.; Wu, L.X.; Ding, Y.F.; Mao, W.F. Microwave Brightness Temperature Anomalies Associated with the 2015 Mw 7.8 Gorkha and Mw 7.3 Dolakha Earthquakes in Nepal. *IEEE Trans. Geosci. Remote Sens.* **2021**. [CrossRef]
24. Qi, Y.; Miao, Z.L.; Wu, L.X.; Ding, Y.F. Seismic Microwave Brightness Temperature Anomaly Detection Using Multitemporal Passive Microwave Satellite Images: Ideas and Limits. *IEEE J. Sel. Top. Appl. Earth Observ. Remote Sens.* **2021**, *14*, 6792–6806. [CrossRef]
25. Ding, Y.F.; Qi, Y.; Wu, L.; Mao, W.F.; Liu, Y.J. Discriminating the Multi-Frequency Microwave Brightness Temperature Anomalies Relating to 2017 Mw 7.3 Sarpol Zahab (Iran-Iraq Border) Earthquake. *Front. Earth Sci.* **2021**, *706*, 656216. [CrossRef]
26. Ulaby, F.T.; David, L. *Microwave Radar and Radiometric Remote Sensing*; The University of Michigan Press: Ann Arbor, MI, USA, 2015.
27. Prigent, C.; Aires, F.; Rossow, W.B. Land surface microwave emissivities over the globe for a decade. *Bull. Am. Meteorol. Soc.* **2006**, *87*, 1573–1584. [CrossRef]
28. Gu, C.M.; Wang, Y.F.; Zhang, X.H.; Zhong, B.; Ma, X.Y. Effects of cloud parameter on brightness temperature computation in microwave band. *J. Appl. Meteor. Sci.* **2016**, *27*, 380–384. [CrossRef]
29. Ulaby, F.T.; Moore, R.K.; Fung, A.K. *Microwave Remote Sensing: Active and Passive. Microwave Remote Sensing Fundamentals and Radiometry*; Artech House: Boston, MA, USA, 1981.
30. Xue, J.J. Characteristics of river silt in the Qaidam Basin, China. *Arid Zone Res.* **2001**, *4*, 44–46. [CrossRef]
31. Zhang, Y.F. Knowledge of several basic characteristics of the geological structures in Qinghai. *Tibetan Plateau Geol. Coll.* **1982**, *3*, 17–27.
32. Kang, W.H. The division and development of tectonic system of the Xizang area. *Tibetan Plateau Geol. Coll.* **1982**, 175–190.
33. 1:1 Million Spatial Databases of Geological Maps of the People's Republic of China. Available online: <http://dcc.ngac.org.cn/geologicalData/rest/geologicalData/geologicalDataDetail/402881f75d9bc10e015d9bc11be70000> (accessed on 14 July 2021).
34. Chen, J.; Chen, J. GlobeLand30: Operational global land cover mapping and big-data analysis. *Sci. China Earth Sci.* **2018**, *61*, 1533–1534. [CrossRef]
35. Imaoka, K.; Kachi, M.; Kasahara, M.; Ito, N.; Oki, T. Instrument performance and calibration of AMSR-E and AMSR2. *Int. Arch. Photog. Remote Sens. Spac. Inf. Sci.* **2010**, *38*, 13–16.
36. Rodell, M.; Houser, P.R.; Jambor, U.E.A.; Gottschalck, J.; Mitchell, K.; Meng, C.J.; Arsenault, K.; Cosgrove, B.; Radakovich, J.; Bosilovich, M.; et al. The global land data assimilation system. *Bull. Am. Meteorol. Soc.* **2004**, *85*, 381–394. [CrossRef]
37. Qin, K.; Wu, L.X.; Zheng, S.; Liu, S.J. A deviation-time-space thermal (DTS-T) method for global Earth observation system of systems (GEOSS)-based earthquake anomaly recognition: Criteria and quantify indices. *Remote Sens.* **2013**, *5*, 5143–5151. [CrossRef]
38. Jin, Y.Q. *Remote Sensing Theory of Electromagnetic Scattering and Thermal Emission*; Science Press: Beijing, China, 1993.
39. Dai, L.C.; Ke, X.; Zhang, F.W.; Du, Y.G.; Li, Y.K.; Guo, X.W.; Li, Q.; Lin, L.; Cao, G.M. Characteristics of hydro-thermal coupling during soil freezing-thawing process in seasonally frozen soil regions on the Tibetan Plateau. *J. Glaciol. Geocryol.* **2020**, *42*, 390–398. [CrossRef]
40. Jing, F.; Singh, R.P. Sensitivity of Land Covers on Passive Microwave Brightness Temperature. In Proceedings of the 2019 IEEE International Geoscience and Remote Sensing Symposium, Yokohama, Japan, 28 July–2 August 2019; pp. 9569–9572.
41. Luo, D.L.; Jin, H.J.; Lin, L.; He, R.X. Degradation of permafrost and cold-environments on the interior and eastern Qinghai Plateau. *J. Glaciol. Geocryol.* **2012**, *34*, 538–546.
42. Freund, F. Toward a unified solid state theory for pre-earthquake signals. *Acta Geophys.* **2010**, *58*, 719–766. [CrossRef]
43. Freund, F. Pre-earthquake signals: Underlying physical processes. *J. Asian Earth Sci.* **2011**, *41*, 383–400. [CrossRef]
44. Mao, W.F.; Wu, L.X.; Liu, S.J.; Gao, X.; Huang, J.W.; Xu, Z.Y.; Qi, Y. Additional microwave radiation from experimentally loaded granite covered with sand layers: Features and mechanisms. *IEEE Trans. Geosci. Remote Sens.* **2020**, *58*, 5008–5022. [CrossRef]
45. Qin, K.; Wu, L.X.; Zheng, S.; Ma, W.Y. Discriminating satellite IR anomalies associated with the MS 7.1 Yushu earthquake in China. *Adv. Space Res.* **2018**, *61*, 1324–1331. [CrossRef]
46. Kleidon, A. *Thermodynamic Foundations of the Earth System*; Cambridge University Press: Cambridge, UK, 2016.